(FeCo/Ppy@C): Pt-free FeCo-Polypyrrole nanocomposites supported on porous carbon for electrochemical application

Francesca Fiorellino, Martina Pilloni, Andrea Ardu, Valentina Cabras, Stefano Columbu, Luisa Russo, Alessandra Scano*, Guido Ennas*

Dipartimento di Scienze Chimiche e Geologiche, Università degli Studi di Cagliari, Cittadella Universitaria di Monserrato, 09042 Monserrato (CA), Italy

*Corresponding author: Tel: (+39) 070 6754381, (+39) 070 6754364; E-mail: alescano80@tiscali.it, ennas@unica.it

DOI: 10.5185/amlett.2019.2203
www.vbripress.com/aml

Abstract

The synthesis and characterization of pyrolyzed carbon-supported transition metal/nitrogen (M–Nx/C) material based on FeCo alloy and Polypyrrol as source of N atoms are presented. Two different synthetic protocols, a multi-step and a novel one pot single-step approach are compared. In both approaches two different Fe:Co ratio (50:50 and 75:25) were used to obtain Pt-free FeCo-Polypyrrole nanocomposites supported on porous carbon (FeCo/Ppy@C). Structural and morphological characterizations of the samples before and after pyrolysis were carried out by using X-Ray Powder Diffracion, Infrared Spectroscopy and High-Resolution Transmission Electron Microscopy. For both approaches, nanoparticles with a core shell structure but different size and matrix polidispersivity were observed after pyrolysis when a Fe:Co 50:50 ratio was used. Bigger nanoparticles were obtained after pyrolysis in the 75:25 ratio samples, with no significant differences between the two approaches. The electrocatalytical properties of the final samples, investigated by cyclic voltammetry in an acidic electrolyte, showed the presence of a cathodic current density.

Keywords: Proton electrolyte membrane fuel cell, non-precious metal catalysts, oxygen reduction reaction (ORR), Pt-free electrocatalysts, conductive polymers, catalytic hydrogen production.

Introduction

Fuel cells have been recognized as clean-energy converting devices. They will play a key role in the reduction of greenhouse gas emissions. Therefore, they are becoming increasingly popular as an alternative to current energy systems, still preponderantly based on fossil fuel reserves. This technology is the key for the transition to a hydrogen-based economy [**1**]. Among the several diverse types of fuel cells under development, the proton electrolyte membrane fuel cell systems (PEMFCs) have attracted the most attention [**2**].

Currently, platinum (Pt)-based carbon-supported catalysts are used in PEMFCs at both the cathode and the anode, hindering their commercialization and large-scale application, due to the high cost of the precious metal Pt and to its limited availability. In 2007 the U.S. Department of Energy (DOE), identified that 56% of the cost of a PEM comes from the platinum-based electrocatalyst. As the sluggish kinetics of the oxygen reduction reaction (ORR) at the cathode requires much more Pt than the faster hydrogen oxidation reaction (HOR) at the anode, its substitution at the cathode would have a significant impact on the PEM final cost. Moreover, platinum-based electrocatalysts cannot meet the 5000 h of operation technical target, resulting in performance losses due to erosion of carbon support, platinum nanoparticle dissolution, poisoning, cathode catalyst oxidation, catalyst migration, membrane degradation and loss of electrode active surface area[2]. Therefore, some approaches have been directed to the production of cheaper catalysts materials, focusing on the cathodic electrode. Some of these new materials showed remarkable high ORR activity with an excellent operational stability. Among the promising electrocatalysts, the non-precious metal catalysts (NPMC) have involved the most part of research interest in the last years [**2-9**]. This recent class of materials, based on transition metals (i.e Cr, Mn, Fe, Co, Ni), includes several types of unsupported or carbon supported electrocatalysts such as macrocycles, conductive polymers, chalcogenides, oxides, carbides and nitrides [**3, 10**].

Martinez *et al.* [**1, 11, 12**] investigated the ORR activity of several conductive polymers in which the nickel and cobalt were incorporated into carbon-supported polypyrrole (Ppy), polyaniline (PANI) or poly 3-methyltiophen (PMeT). These polymers were

considered ideal as electrocatalysts due to their high electroconductivity, redox properties and low cost. It was found that the presence of heteroatoms as N, which is an electron donor (in the case of Ppy and PANI) provided a better ORR activity than sulphur atoms (PMeT). Other studies showed an improved ORR catalytic activity by adding the transition metal Ni, while the addition of Co improved the ORR performance and stability [**3**].

Although preliminary investigations on pyrolyzed NPMC had indicated that the higher ORR activity was achieved when Fe and Co were used as separate component [**13**], Zelaney *et al.* successfully synthesized a pyrolyzed carbon supported Co/Fe- PANI electrocatalyst with a superior performance ascribed directly to the metal combination [**14**]. According to Zelaney *et al.*, the presence of Fe determines the high ORR activity of electrocatalyst meanwhile the Co improves its stability. Therefore, the idea of combining Fe and Co in a composite electrocatalyst has inspired several studies reported in literature [**3, 15-18**] as well as the present study. We propose the synthesis and characterization of pyrolyzed carbon-supported transition metal/nitrogen (M–Nx/C) material[3] based on FeCo alloy [**19, 20**] and Ppy as source of N atoms. The experimental part describes two different synthetic protocols: a multi-step approach, which reflects the ones reported in literature [**14**] (applied by the authors with some modification), and a novel one pot single-step approach developed by the authors. We tried to explain the effect of the two different approaches in the structural and morphological properties of the final samples. The samples were prepared using different Fe/Co nominal molar ratio starting from nitrate metal salts as cheap precursors.

The electrocatalytical properties of the final samples were also investigated. Differently from most of the studies reported in literature, the final samples were subjected to a leaching process in H_2SO_4 aqueous solution for 8 hours to verify the stability of the catalyst before the investigation by cyclic voltammetry in acidic electrolyte. In fact, it is well known that the metallic components of such NPMC dissolve during time in this strong acidic condition. This effect is responsible of the observed decay of ORR in PEMFCs after a few hours.

Experimental

Chemicals

The syntheses were carried out using the following reagents with the purity grade commercially available and without any further purification: Pyrrole (Sigma Aldrich, 98%), $Fe(NO_3)_3{\cdot}9H_2O$ (Riedel-de Haen, ≥98%), $Co(NO_3)_2{\cdot}6H_2O$ (Sigma Aldrich, 98%), carbon black (Strem Chemicals, SSA1300-1400 m^2/g), H_2SO_4 (Sigma-Aldrich, 98%).

For the electrochemical measures the Nafion® solution (5 wt %) and the H_2SO_4 (98%) were purchased from Sigma-Aldrich and ethanol (96%, ACS grade) from J.T. Baker.

Material synthesis

In this research the samples were obtained by two different approaches, a multi-step and a single-step approach labelled here as Protocol A and Protocol B respectively.

***Protocol A*:** in a four-neck round bottom flask in an ice bath, under Ar flow, 3.8 mL of pyrrole were added to 98.2 mL of fresh bidistilled water and stirred for 10 minutes before to add by drops 10 mL of an 0.125 M aqueous solution of $Fe(NO_3)_3{\cdot}9H_2O$. The resulting mixture was still stirred and protected from light exposure for 3h to achieve the pyrrole polymerization. After 3h, 2 g of carbon black was added, and 10 mL of an aqueous solution of $Co(NO_3)_2{\cdot}6H_2O$ were dropped into the flask. The suspensions were kept under stirring for 12h. Successively, the water was almost removed using a rotavapour and a dark paste was collected and dried at 50 °C under vacuum overnight. Two samples with different Fe/Co nominal molar ratio (see details in **Table 1**) were prepared according to this procedure simply changing the concentration of Co^{2+} solution. The sample A-50 was obtained using a 0.125M solution of cobalt nitrate while the sample A-75 was obtained with a 0.041M solution. These samples were then pyrolyzed in a home-made tubular oven up to 800°C for 4h under Ar atmosphere. The samples after pyrolysis were labelled A-50P and A-75P. A process of leaching with a 0.5M H_2SO_4 aqueous solution at 80°C was applied to the pyrolyzed samples for 8h, and the samples A-50L and A-75L were thus obtained.

***Protocol B*:** 20 mL of an aqueous solution contained iron and cobalt nitrate were added by drops in a four-neck round bottom flask containing 3.8 mL of pyrrole, 96.2 mL of distilled water and 2 g of carbon black under stirring in an ice bath and under Ar flow. After the complete addition of the salt solution, the mixture was kept stirring and protected from the light for other 12h. Later, water was removed from the mixture by evaporation using a rotavapor, and a fine black powder was obtained after 12h at 50 °C under vacuum. Two samples, B-50 and B-75, with different Fe/Co nominal molar ratio (**Table 1**) were prepared using this procedure and varying the concentration of cobalt nitrate in the aqueous solution. The samples B-50P and B-75P were then obtained by pyrolysis (800 °C for 4h in Ar atmosphere). Finally, the pyrolyzed samples were leached in sulfuric acid as previously described, and the samples B-50L and B-75L were obtained.

Table 1. Nominal composition of the samples obtained in this work using *Protocol A* and *Protocol B*.

Sample	Fe:Co molar ratio (%)	Approach	(Fe+Co) wt% / total
A-50	50:50	Multistep	2.46%
A-75	75:25	Multistep	1.63%
B-50	50:50	Single-step	2.46%
B-75	75:25	Single-step	1.63%

Characterization

X-Ray Powder Diffraction (XRPD) patterns were collected with a Seifert X3000 diffractometer (Ahrensburg, Germany) operating at 35 mA and 40 kV using Cu Kα radiation and equipped with a graphite monochromator on the diffracted beam. Patterns were recorded in a step scan mode in the range $5° \leq 2\vartheta \leq 80°$ with a step size of 0.05 2ϑ degree, collecting at least 1000 counts for each step. Samples were deposited on the silicon zero background sample holder. Precise lattice determination and average crystalline size were carried out using Maud program [**21**] where the instrumental correction broadening was derived from fitting of the XRPD data obtained from standard samples [**22**].

High resolution transmission electron microscopy (HRTEM) was also used to characterized the samples. The analysis was carried out by using a JEM 2010 UHR equipped with a Gatan Imaging Filter (GIF) with a 15eV window and a slow scan CCD camera. For the HRTEM observations, samples were dispersed in octane, submitted to an ultrasonic bath and the suspension was then dropped on carbon coated copper grids.

To confirm the polymerization of pyrrole into polypyrrole, FTIR analysis was performed using a Bruker Tensor 27 spectrophotometer, equipped with a diamond-ATR accessory and a DTGS detector. A number of 128 scans at a resolution of 2 cm^{-1} were averaged from wave number 4000 to 400 cm^{-1}.

Electrochemical measures

The electrocatalytical properties of the samples after leaching were measured by a Cyclic Voltammetry (CV, Autolab PGSTAT 128N Metrohm) at room temperature in air atmosphere, at the potential range 0 - 1 V and with a scan rate of 0.1 mV/s. The CV measurements were performed using a typical three-electrode system. In the middle of the system, a working electrode (WE) is placed, on the right hand a platinum counter electrode is positioned, while on the left hand the reference electrode (RE) Ag/AgCl is positioned. A mixed aqueous solution containing 0.5M H_2SO_4 and 100 mM NaCl was used as electrolyte. To prepare the working electrode (WE), 4mg of the catalyst was ultrasonically suspended in 2 mL of ethanol and 10μL of Nafion® solution for 30 min to obtain a well dispersed ink. The experiments were conducted using 40 drops of ink on the WE.

Results and discussion

The series of NPMC containing Fe and Co supported on a N-modified carbon matrix were prepared through two different protocols. In the *Protocol A*, based on a multi-step approach, the synthesis started with the polymerization of pyrrole [**23**], followed by the impregnation of the metal precursors and the N-polymer on the active carbon. On the other hand, the *Protocol B* followed a one pot single step approach in which the polymerization and impregnation occurred together.

The XRPD patterns of the as prepared samples (**Figs. SI1** and **SI2**) show a difference between 50:50 and 75:25 samples. In fact, very well defined XRPD peaks are observed in the 50:50 samples (A-50 and B-50) due to the presence of crystallites of iron nitrate hydrated while a very disordered structure is observed in the case of 75:25 samples (A-75 and B-75). However, no relevant differences can be noticed between the samples obtained by *Protocol A* and *Protocol B*.

The polymerization of pyrrole into polypirrole was confirmed by FTIR spectra (not reported), which agree with the data reported in literature [**24**].

A pyrolysis treatment was performed in order to obtain the metallic alloy FeCo, to incorporate the N atoms into the carbon matrix and to generate C-N species (A-50P and B-50P samples) [**5**].

The XRPD patterns of samples 50:50 ratio after pyrolysis are reported in **Fig. 1a**. In both patterns, the prominent peaks are assigned to bcc- phase (card 44-1433) [**25**]. This result indicates that under the thermal treatment the formation of metallic alloy was effectively achieved. The cell parameter a_0 corresponds to 2.857 Å in agreement with the reported values of microcrystalline Wairauite [**26**]. An estimation of the crystallite dimensions by Rietveld analysis reveals crystallites with an average size of 110nm for A-50P, and smaller crystallites of 57 nm for the B-50P sample. Minor peaks due to the $CoFe_2O_4$ phase (card 03-0864) [**25**] are detectable in both patterns (**Fig. 1a**). Under pyrolysis, the formation of the metallic particles from the nitrates evolves throughout the processes of hydrolysis, dehydration and finally reduction. Mixed oxides are formed as intermediate phases. This explains the presence of cobalt ferrite in the samples and suggests an incomplete reduction into FeCo during the pyrolysis.

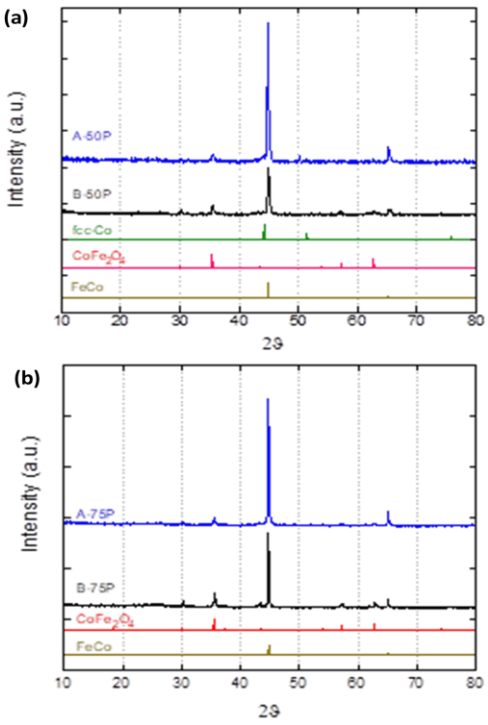

Fig. 1. (a) XRPD patterns of the A-50P and B-50P (pyrolyzed) samples. fcc-Co, $CoFe_2O_4$ and FeCo reference data are also reported. (b) XRPD patterns of the A-75P and B-75P (pyrolyzed) samples. $CoFe_2O_4$ and FeCo reference data are also reported.

In the A-50P sample, the calculated cell parameters for the cubic $CoFe_2O_4$ phase is 8.386 Å with an average size dimension of 44 nm, while for the B-50P, the cell parameter is 8.388 Å with an average size of 49 nm. Traces of fcc α-Co and a cubic primitive ε-Co [**27**] are also visible in **Fig. 1a**, particularly in the A-50P sample.

Fig. 1b shows the XRPD patterns of the A-75P and B-75P samples. The FeCo alloy is the main phase formed during the thermal treatment at 800°C like in the samples in **Fig. 1a**. However, the reduction was not completed, in fact the peaks at 35.5° and 62.7° 2θ revel the presence of $CoFe_2O_4$ phase. The cell parameter (a_0) calculated for the alloy phase in A-75P and B-75P corresponds to 2.869 Å. This value is very close to 2.863 Å which is the a_0 of microcrystalline $Fe_{70}Co_{30}$ phase [**28, 29**]. The average crystallites size is around 120 nm for both samples. It is noteworthy that the FeCo alloy obtained from the samples with 75:25 Fe:Co molar ratio, exhibits bigger crystallites than those obtained from the samples with 50:50 molar ratio. This difference is related to the bcc lattice alloy crystal growth, where cobalt is substitutionally inserted in the α–Fe structure. Therefore, the crystal growth is favoured by higher content of iron.

The XRPD analysis does not reveal the presence of metallic carbide (M-C) or another M-N mixed crystalline phases.

Fig. 2 and **3** show the HRTEM images at different magnification for the A-50P and B-50P samples. In both cases, the images depict spherical nanocrystalline particles well dispersed in a non-crystalline matrix. It should be noted that B-50P sample exhibits smaller nanoparticles with a better dispersion in the matrix than the A-50P sample. This observation could be correlated with the synthetic approach used for the synthesis of the as prepared samples. It is possible to assume that the single-step procedure (*Protocol B*) determined a more homogenous dispersion of the precursors into the matrix, which defines the better dispersion of the metallic alloy nanoparticles. It is noteworthy the role of the matrix which prevents the coalescence of the nanoparticles during the thermal treatment.

The nanoparticles of A-50P and B-50P samples display a typical core-shell structure already observed for similar samples [**29**].The calculation of d-spacing of selected areas (SAED) reveals the presence of $CoFe_2O_4$ phase in the shell with the plane (311), while the FeCo alloy is narrowed in the core. The presence of these phases confirms the XRPD analysis previously discussed. Furthermore, in **Fig. 3c** fringes are observed at distance of 1.96 and 2.08 Å, due to the (101) and (012) planes of a graphitized carbon phase (card 26-1079) [**25**]. However, this phase was not clearly visible in the XRPD patterns of pyrolyzed samples (**Fig. 1**). The graphitization of amorphous carbon is a process that occurs in presence of metallic species at high temperature [**30**-**35**]. In this case, the metallic particles, obtained during the heat treatment at 800 °C of 4h, were able to catalyze the formation of graphite from the carbonaceous matrix in which they were dispersed.

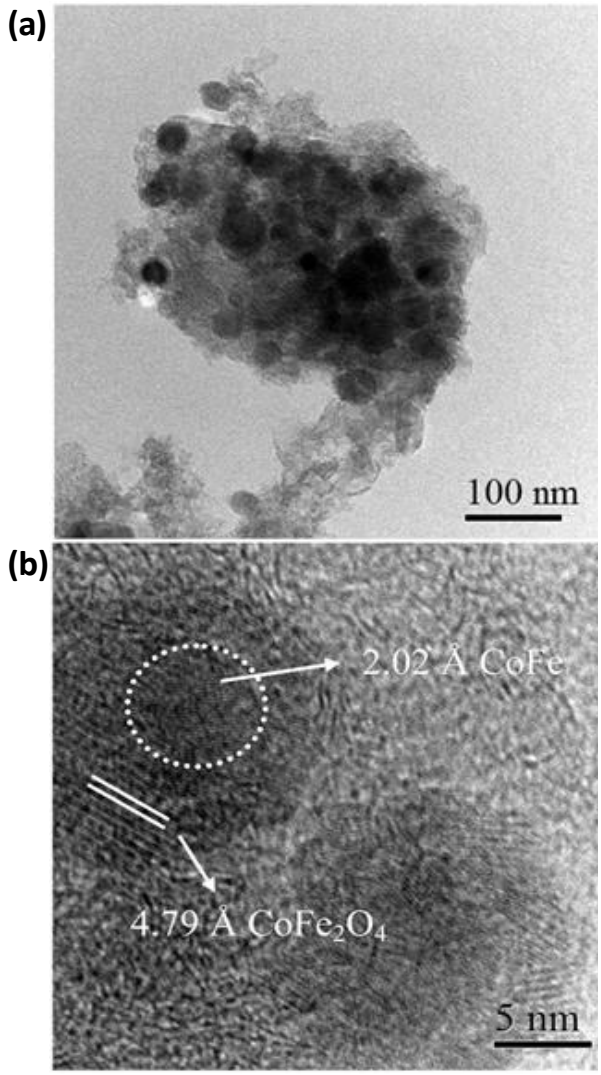

Fig. 2. (a) low magnification and (b) high resolution TEM images of the A-50P sample.

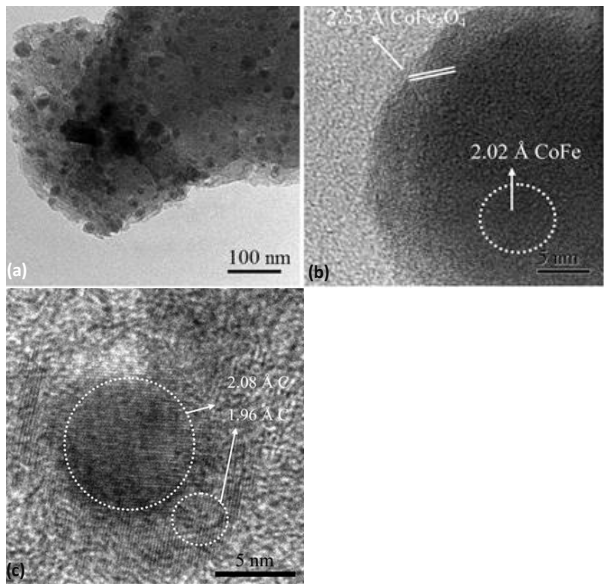

Fig. 3. TEM micrographs of the B-50P sample. (a) Overview, (b) detail of the core-shell structure and (c) detail of the graphitic phase.

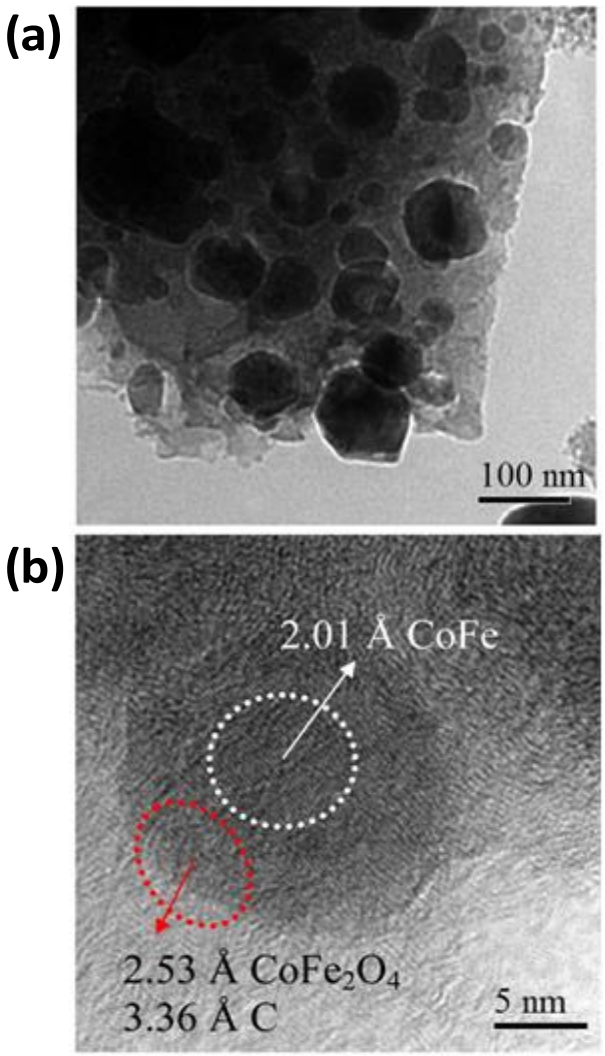

Fig. 4. TEM micrographs of the A-75P sample. (a) Low magnification and (b) a detail of the core-shell structure.

The presence of the graphitized carbon (**Fig. 4b**) was also spotted in the pyrolyzed samples with 75:25 ratio. No significant differences were observed between the A-75P and B-75P samples. In fact, both displayed spherical nanoparticles with a core-shell structure not homogenously dispersed into the matrix (**Fig. 4a**).

The HRTEM results allowed some additional consideration concerning the two different synthetic approaches (*Protocol A* and *B*), and the two different molar ratios used in this study. Overall, the samples with 50:50 ratio gave after pyrolysis smaller spherical nanoparticles than the samples 75:25. The protocol used for the preparation of the as prepared samples seems to influence the final size and dispersion of the metal alloy nanoparticles. In fact, the sample 50:50 obtained by *Protocol B*, showed smaller nanoparticles with a better dispersion in the matrix in comparison to the sample obtained by *Protocol A*. For this reason, the single step approach appears to be the best one for preparing the samples with 50:50 molar ratio. This was not observed in the case of 75:25 ratio where the presence of higher amount of iron favours the crystal growth and increases the polydispersivity.

The treatment with sulfuric acid at 80°C was carried out to test the stability of the pyrolyzed samples. An amorphous matrix with cavities was observed under HRTEM analysis (**Fig. 5**). The absence of $CoFe_2O_4$ and FeCo phase in the leached samples was confirmed by XRPD patterns (SI3), which show an amorphous halo centered around 26° 2θ and a peak at 26.6° 2θ of a graphitic structure in analogy with previous studies[5]. Minor peaks due to FeOOH goethite phase were also observed in the XRPD pattern (card 29-713) [**25**]. Goethite is produced during the leaching when Fe^{3+} ions, resulting from FeCo and $CoFe_2O_4$, undergo to chemical precipitation in 0.5M H_2SO_4 aqueous solution at 80 °C. This result points out that the nanoparticles were not enough protected by the carbonaceous matrix.

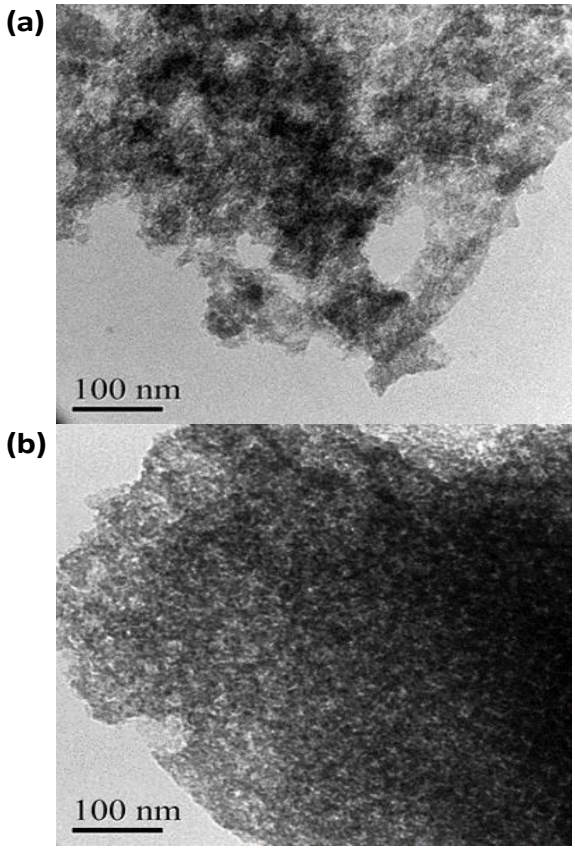

Fig. 5. TEM micrographs of A-50L (a) and B-50L (b) samples.

Electrocatalytic activity

A preliminary electrocatalytical characterization of the best samples from the morphological and structural point of view, was performed by cyclic voltammetry. In the CV experiment (**Fig. 6**), A-50L and B-50L samples show a very similar profile. A low cathodic current density with a broad peak around 0.4 V while a faint anodic peak at 0.4 V was observed. The presence of this weak ORR activity permits to highlight the presence of electroactive species even if at low concentration. To explain this result different speculations can be made. The catalytic activity could be attributed to some residual extremely dispersed or amorphous metallic nanoparticles, which endured the leaching process. On the other hand, it is not

possible to exclude the presence of electroactive metal free N–C species[3].

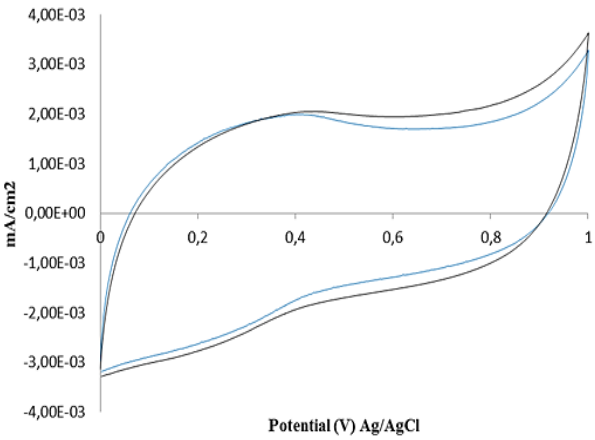

Fig. 6. CV plot of the B-50L (black) and A-50L (blue) samples after pyrolysis and leaching treatments.

Conclusion

Two different approaches for the preparation of pyrolyzed carbon-supported transition metal/ nitrogen (M–Nx/C) material for ORR have been presented. The samples were prepared using two different Fe:Co molar ratio. The samples after pyrolysis showed the formation of $Fe_xCo_{(100-x)}$ alloy as main phase. In the case of 50:50 ratio, the samples obtained with different approaches showed (after pyrolysis) nanoparticles with the same core shell structure but with different size and polidispersivity in the matrix. In the case of sample obtained by single-step approach, the FeCo alloy showed crystallites of 57 nm (average size). When using the 75:25 ratio, bigger nanoparticles were always obtained after pyrolysis, but not significant differences were observed between A- and B- samples.

It was displayed that the nanoparticles were not enough protected by the carbonaceous matrix and they were removed from the carbonaceous matrix after 8 hours of acidic leaching process.

Preliminary studies on ORR activity carried out on the A-50L and B-50L samples showed still the presence of a slightly activity. Future studies are necessary to investigate which species are responsible of this activity.

Acknowledgements

The authors thank the Dipartimento di Scienze Chimiche e Geologiche, Università degli Studi di Cagliari for the financial support: FIR 2017 and FIR 2018, "Progetti biennali d'Ateneo – Fondazione di Sardegna/Regione Autonoma della Sardegna" 2016-17.

Author's contributions

Conceived the plan: mp, as, ge; Performed the expeirments: lr, ff, aa, mp; Data analysis: vc, sc, mp, as, ge; Wrote the paper: ff, mp, as, ge. Authors have no competing financial interests.

Supporting information

Supporting informations are available from VBRI Press.

References

1. Martínez Millán, W.; Toledano Thompson, T.; Arriaga, L. G.; Smit, M. A., *Int. J. Hydrogen Energy* **2009**, *34*, 694.
2. Othman, R.; Dicks, A. L.; Zhu, Z., *Int. J. Hydrogen Energy* **2012**, *37*, 357.
3. Chen, Z.; Higgins, D.; Yu, A.; Zhang, L.; Zhang, J., *Energy Environ. Sci.* **2011**, *4*, 3167.
4. Banham, D.; Ye, S.; Pei, K.; Ozaki, J. I.; Kishimoto, T.; Imashiro, Y.;, *J. Power Sources* **2015**, *285*, 334.
5. Domínguez, C.; Pérez-Alonso, F. J.; Abdel Salam, M.; Gómez De La Fuente, J. L.; Al-Thabaiti, S. A.; Basahel, S. N.; Peña, M. A.; Fierro, J. L. G.; Rojas, S., *Int. J. Hydrogen Energy* **2014**, *39*, 5309.
6. Bashyam, R.; Zelenay, P., *Nature* **2006**, *443*, 63.
7. Brouzgou, A.; Song, S. Q.; Tsiakaras, P., *Appl. Catal. B Environ.* **2012**, *127*, 371.
8. Li, X.; Popov, B. N.; Kawahara, T.; Yanagi, H., *J. Power Sources* **2011**, 196, 1717.
9. Higgins, D. C.; Chen, Z.; Can. J., *Chem. Eng.* **2013**, *91*, 1881.
10. Bezerra, C. W. B.; Zhang, L.; Lee, K.; Liu, H.; Marques, A. L. B.; Marques, E. P.; Wang, H.; Zhang, J., *Electrochim. Acta* **2008**, *53*, 4937.
11. Sulub, R., *Int. J. Electrochem. Sci* **2009**, *4*, 1015.
12. Smith, A. L., The Coblentz Society Desk Book of Infrared Spectra. **1982**.
13. Morozan, A.; Jousselme, B.; Palacin, S., *Energy Environ. Sci.* **2011**, *4*, 1238.
14. Wu, G.; More, K. L.; Johnston, C. M.; Zelenay, P., *Science*. **2011**, *332*, 443.
15. Liu, Q.; Cao, S.; Qiu, Y., *Int. J. Hydrogen Energy* **2017**, *42*, 29274.
16. Scofield, M. E.; Liu, H.; Wong, S. S., *Chem. Soc. Rev.* **2015**, *44*, 5836.
17. Zhang, H. J.; Yuan, X.; Sun, L.; Yang, J.; Ma, Z. F.; Shao, Z., *Electrochim. Acta* **2012**, *77*, 324.
18. Shui, H.; Jin, T.; Hu, J.; Liu, H., ChemElectroChem **2018**, *5*, 1401.
19. Falqui, A.; Serin, V.; Calmels, L.; Snoeck, E.; Corrias, A.; Ennas, G., *Journal of Microscopy* **2003**, *210*, 80.
20. Ennas, G.; Marongiu, G.; Marras, S.; Piccaluga, G., *J. Nanoparticle Res.* **2004**, *6*, 99.
21. Lutterotti L.; Matthies S.; Wenk HR., *Newsl. CPD* **1999**, *21*, 14.
22. Young R., The Rietveld Method; Oxford University Press, Ed.; Oxford, **1993**.
23. Armes, S. P., Synth. Met. **1987**, *20*, 365.
24. Tian, B.; Zerbi, G., *J. Chem. Phys.* **1990**, *92*, 3886.
25. PDF File. JCPDS International Center for Diffraction Data, 1601 Park Lane, Swarthmore, PA.
26. Bayliss, P. SovrMnrns. **1990**, *28*, 751.
27. Sun, S.; Murray, C. B., *J. Appl. Phys.* **1999**, *85*, 4325.
28. Ennas, G.; Falqui, A.; Paschina, G; Marongiu, G., *Chem. Mater.* **2005**, *8*, 6486.
29. Ennas, G.; Falqui, A.; Marras, S.; Sangregorio, C.; Marongiu, G., *Chem. Mater.* **2004**, *16*, 5659.
30. Sevilla, M.; Fuertes, A. B., Carbon N. Y. **2006**, *44*, 468.
31. Oya, A.; Marsh, H., *J. Mater. Sci.* **1982**, *17*, 309.
32. Yudasaka, M.; Tasaka, K.; Kikuchi, R.; Ohki, Y.; Yoshimura, S.; Ota, E., *J. Appl. Phys.* **1997**, *81*, 7623.
33. Marsh, H.; Crawford, D.; Taylor, D. W., *Carbon N.Y.* **1983**, *21*, 81.
34. OP Krivoruchko, V. Z., *Kinet. Catal*. **1998**, *39*, 561.
35. Oberlin, A.; Rouchy, J. P., *Carbon N.Y.* **1971**, *9*.

Supporting Information

Fig. SI1 shows the XRPD patterns of the A-50 and B-50 samples before pyrolysis in Ar at 800 °C for 4h. The samples obtained with the two different approaches, show clear peaks corresponding to $Co(NO_3)_2 \cdot 6H_2O$, indicating the formation of a mixed iron cobalt nitrate phase.

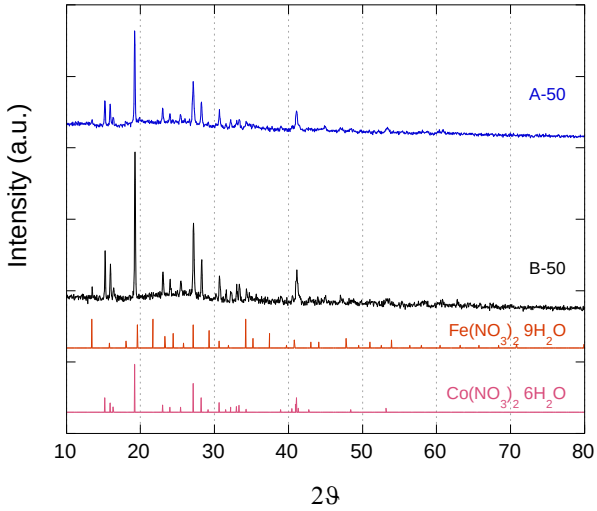

Fig. SI1. XRPD of the A-50 and B-50 samples before pyrolysis. $Fe(NO_3)_3 \cdot 9\ H_2O$ and $Co(NO_3)_2 \cdot 6\ H_2O$ reference data are also reported.

Fig. SI2 shows the XRPD patterns of A-75 and B-75 (Fe:Co 75:25 molar ratio) before the heat treatment. In the XRPD pattern of the samples, it is evident that iron and cobalt nitrates give rise to the formation of amorphous material. The peaks corresponding to nitrates are not clearly visible; on the contrary they were evident in the samples with molar Fe:Co ratio 50:50. Presumably, this is due to a better dispersion of nitrates in the matrix in samples with molar Fe:Co ratio 75:25.

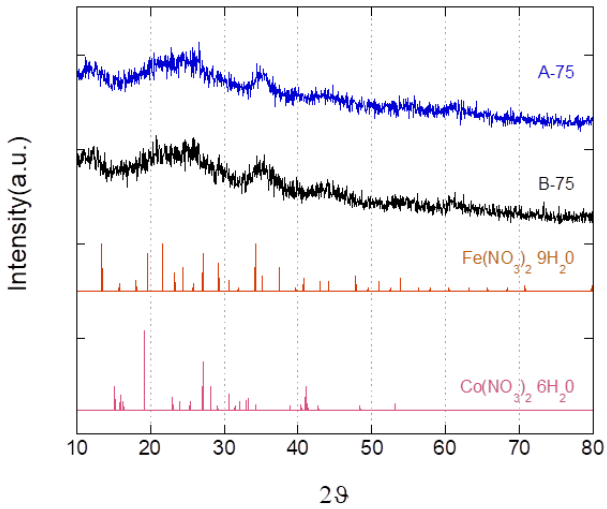

Fig. SI2. XRPD of A-75 and B-75 samples before pyrolysis. $Fe(NO_3)_3 \cdot 9\ H_2O$ and $Co(NO_3)_2 \cdot 6\ H_2O$ reference data are also reported.

(a)

(b)

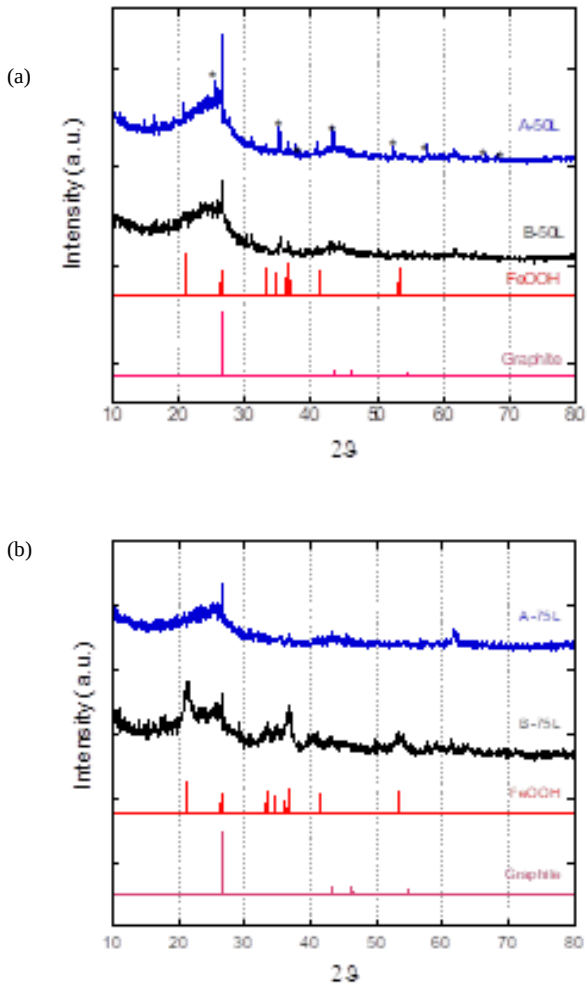

Fig. SI3a and SI3b. XRPD of A-50L and B-50L samples (SI3a) and XRPD patterns of the A-75L and B-75L samples (SI3b).

Fig. SI3a shows the XRPD patterns of the A-50L and B-50L samples. Graphite reference data are also reported. *indicates the α-Al_2O_3 peaks due to the support. **Fig. SI3b** shows the XRPD patterns of the A-75L and B-75L samples. Graphite and Goethite (FeOOH) reference data are also reported. Goethite, produced during the leaching of FeCo and $CoFe_2O_4$ phases, undergoes to chemical precipitation in 0.5M H_2SO_4 aqueous solution at 80 °C.